Pergamon

Int. J. Solids Structures Vol. 33, No. 29, pp. 4293–4307, 1996

0020–7683/96 $15.00 + .00

0020–7683(95)00240–5

COMPUTING STRAIN FIELDS FROM DISCRETE DISPLACEMENT FIELDS IN 2D-SOLIDS

M. G. D. GEERS,† R. DE BORST‡ and W. A. M. BREKELMANS
Faculty of Mechanical Engineering, Eindhoven University of Technology, Eindhoven, The Netherlands

(*Received* 18 *July* 1995; *in revised form* 3 *October* 1995)

Abstract—The analysis of strain localization and damage evolution in materials requires appropriate experimental techniques to verify the complex material behaviour in the damaging zone. Modern techniques are now available to measure the displacement fields in small zones of a material, and a complementary procedure is needed to derive the accompanying strain fields. The knowledge of the local strain fields gives direct information with respect to the applied constitutive model and serves as initial input for most parameter estimation procedures, while the fine-tuning of the model parameters should be done by comparing the computed and measured displacement fields. This study presents a theory to compute strains from the displacements in a discrete set of points and is particularly useful in the post-processing of experimentally measured displacement fields. The theory is fully elaborated, and some practical examples are given. A comparison is made with some analytical solutions, and the effect of noise on the input data is evaluated. Copyright © 1996 Elsevier Science Ltd.

1. INTRODUCTION

In recent years, it has been recognized that the mathematically consistent description of failure and the accompanying localization phenomenon requires higher-order continuum models or the addition of viscosity in the constitutive description (for an overview see, for instance, de Borst *et al.*, 1993). If such an enhancement is not made, ill-posed boundary value problems result, which cannot properly represent the physical failure process. The quoted remedy, namely the introduction of higher-order continuum descriptions, invariably introduce one or more additional material parameters, the number depending on the type of enhancement (non-local, gradient or micro-polar continua) or the specific constitutive setting (e.g., damage or plasticity). In any case a material parameter is introduced that has the dimension of length, and which is related to the dimensions of the localization zone.

A problem now resides in the determination of this characteristic length, since it cannot be measured via simple tests, in which one tries to achieve uniformity of the specimen. Evidently, homogenous deformations do not trigger strain gradients, and the higher-order deformation terms then vanish, and so does the influence of the characteristic length parameter. Accordingly, the proper determination of the characteristic length parameter can only be carried out for non-uniform tests, whereby the size and the strain distribution in the localization zone are determined accurately by local measurements, and subsequently compared with the results of numerical simulations using a specific enhanced damage or plasticity model.

Experimental techniques that can measure locally are often based on optical methods, e.g. the Electronic Speckle Pattern Interferometry ESPI (Bergmann *et al.*, 1995; Galanulis and Ritter, 1993), or the Hentschel Random Access Tracking System (Zamzow, 1990). Alternatively, length transducers or magnetic resonance imaging can be used, e.g. the measurement of strain fields in the walls of the heart (Hunter and Zerhouni, 1989). These methods provide information of the displacements at discrete points on the surface of the body, and are therefore well-suited for relatively thin structures. However, in continuum mechanics-based theories such as continuum damage mechanics (CDM) knowledge of the strains is often required, e.g., for the determination of threshold levels of damage.

† Also at Faculty of Civil Engineering, RMA, Brussels, Belgium.
‡ Also at Faculty of Civil Engineering, Delft University of Technology, Delft, The Netherlands.

For the determination of strains on basis of these experimentally acquired displacement data (Peters, 1987) has presented a method in which the local differences in the displacements have been expanded in a Taylor series, which was truncated after the first, linear term. While giving good results for slowly varying strain fields, this method is insufficient in the presence of steep strain gradients, or near edges, either external, or internal (cracks). For the accurate determination of strains on the basis of discrete displacements an improved method is called for, which is the subject of this contribution. After outlining the notation used in this study, the improved method will be derived in detail. Next, an accuracy assessment will be given of the method presented by Peters (1987) and the approach developed here. Attention will also be given to the possible effect which corrupted data may have on the accuracy.

2. NOTATIONS AND CONVENTIONS

Throughout the theoretical elaborations the following notations will be used, with their definition in a Cartesian coordinate system between parentheses:

Scalar	$\Rightarrow a$	
Vector	$\Rightarrow \mathbf{a}$	$(= a_i)$
Second-order tensor	$\Rightarrow \mathbf{A}$	$(= A_{ij})$
Third-order tensor	$\Rightarrow {}^3\mathbf{A}$	$(= A_{ijk})$
Fourth-order tensor	$\Rightarrow {}^4\mathbf{A}$	$(= A_{ijkl})$
Dyadic product	$\Rightarrow \mathbf{AB}$	$(= A_{ij}B_{kl})$
Inner product	$\Rightarrow \mathbf{A}\cdot\mathbf{B}$	$(= A_{ij}B_{jk})$
Double inner product	$\Rightarrow \mathbf{A}:\mathbf{B}$	$(= A_{ij}B_{ji})$
Triple inner product	$\Rightarrow {}^3\mathbf{A}\vdots{}^3\mathbf{B}$	$(= A_{ijk}B_{kji})$
Quadruple inner product	$\Rightarrow {}^4\mathbf{A}::{}^4\mathbf{B}$	$(= A_{ijkl}B_{lkji})$
Inversion	$\Rightarrow \mathbf{A}^{-1}$	
Conjugation	$\Rightarrow \mathbf{A}^c$	$(A^c_{ijkl} = A_{lkji})$
Estimate of a tensor	$\Rightarrow \hat{\mathbf{A}}$	
Finite difference	$\Rightarrow \Delta$	

The theoretical elaborations in the next section are entirely based on a 2D-continuum, deformed in its plane. The behaviour of the material is characterised by the displacements of a discrete set of points at the surface of the material. The material coordinates, representing the initial configuration at time $t = 0$ of the representative particles of the continuum, are designated with upper-case letters or $\mathbf{X}$ in vector notation. The spatial coordinates, representing the configuration at time t, are designated with lower-case letters or $\mathbf{x}$, in vector notation. The coordinate systems for material and spatial coordinates are considered to be superimposed with rectangular Cartesian coordinate axes. At time $t = 0$, $\mathbf{X}$ may then be written as

$$\mathbf{X} = \mathbf{x}_0. \tag{1}$$

Using this coordinate systems all material coordinates will now be denoted by their spatial coordinates at time $t = 0, \mathbf{x}_0$.

3. FORMULATION OF THE METHOD

3.1. *Gradient deformation formulation*

Consider two neighbouring particles, which occupy the points P_0 and Q_0 in the plane 2D-continuum at time $t = 0$. The position vector of P_0 is identified by $\mathbf{x}_0$ while the position

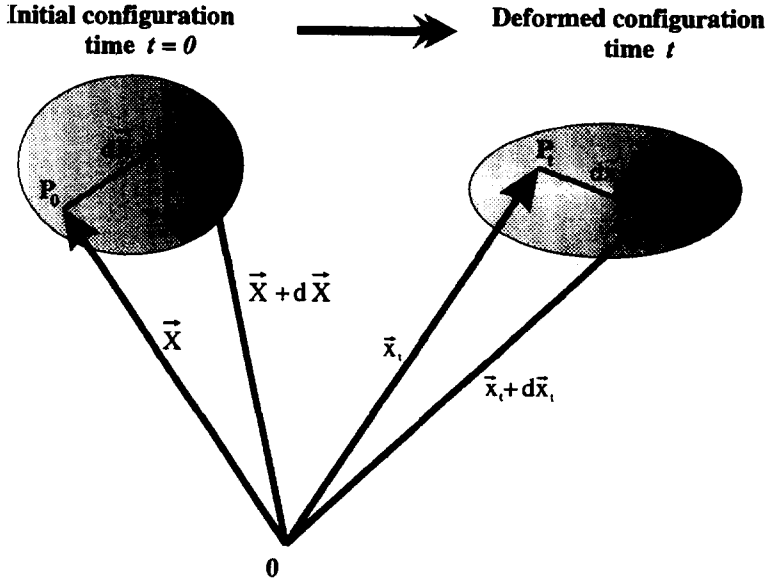

Fig. 1. Infinitesimal deformation in the 2D-plane.

vector of Q_0 can be written as $\mathbf{x}_0+\mathrm{d}\mathbf{x}_0$. At time t, after deformation, the two particles move to the points P_t and Q_t identified by $\mathbf{x}_t$ for P_t and $\mathbf{x}_t+\mathrm{d}\mathbf{x}_t$ for Q_t (Fig. 1).

The deformation tensor in P_t at time t is now defined as:

$$\mathrm{d}\mathbf{x}_t = \mathbf{F}\cdot\mathrm{d}\mathbf{x}_0 \tag{2}$$

which results in

$$\mathbf{F} = (\nabla_0\mathbf{x}_t)^c = \frac{\partial \mathbf{x}_t}{\partial \mathbf{x}_0}.$$

At a fixed time t the actual position vector $\mathbf{x}_t$ of a point P_t can be considered as a function of the initial position vector $\mathbf{x}_0$. The position vector of a neighbouring point $\mathbf{x}_t+\Delta\mathbf{x}_t$ can be written as a vectorial Taylor-series expansion, truncated after the second-order terms:

$$\Delta\mathbf{x}_t = \frac{\partial \mathbf{x}_t}{\partial \mathbf{x}_0}\cdot\Delta\mathbf{x}_0 + \frac{\partial^2\mathbf{x}_t}{\partial \mathbf{x}_0^2}:\Delta\mathbf{x}_0\Delta\mathbf{x}_0 + \mathbf{a} \tag{3}$$

where $\mathbf{a}$ represents the theoretical discretization (or truncation) error. Equation (3) involves the deformation tensor $\mathbf{F} = \partial\mathbf{x}/\partial\mathbf{X}$ (eqn (2)) and the gradient deformation tensor $\partial^2\mathbf{x}/\partial\mathbf{X}^2$ of rank three. The tensor ${}^3\mathbf{G}$ is defined as:

$${}^3\mathbf{G} = \tfrac{1}{2}\frac{\partial^2\mathbf{x}}{\partial\mathbf{X}^2}.$$

Using this definition eqn (3) can be rewritten:

$$\Delta\mathbf{x}_t = \mathbf{F}\cdot\Delta\mathbf{x}_0 + {}^3\mathbf{G}:\Delta\mathbf{x}_0\Delta\mathbf{x}_0 + \mathbf{a}. \tag{4}$$

Consider the central particle at the point P_t surrounded by k neighbouring particles at

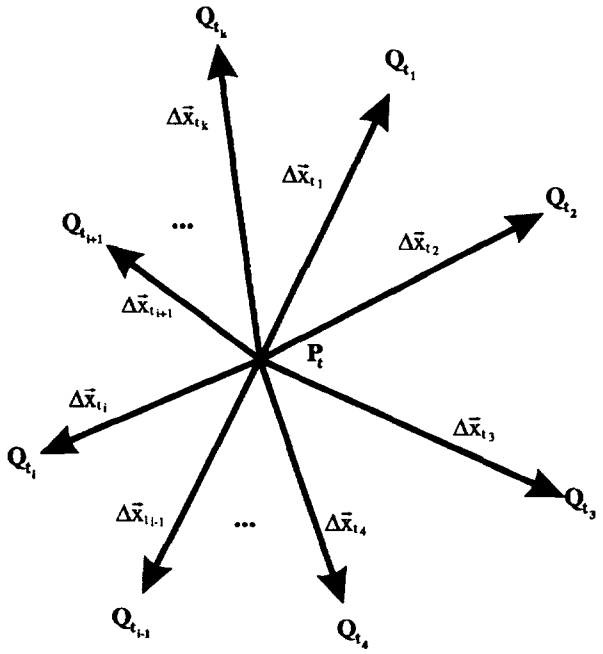

Fig. 2. Particle distribution around the central point.

the points Q_{t_i} (Fig. 2). Equation (4) can now be formulated for each point Q_{t_i} involving a discretization error $\mathbf{a}_i$ for each equation. These errors $\mathbf{a}_i$ can be decomposed in a constant average error (for the group of particles in consideration) $\mathbf{a}$ and a variable error $\delta\mathbf{a}_i$, determined by the exact position Q_{t_i} of each particle. It is assumed that this variable error is random and follows a normal distribution (the error is tied to the scattered positions of the particles around their mean positions). At least six particles at Q_{t_i} are required to solve the unknowns in the eqn 4 and thus to determine an estimation for F in P_t. If more than six particles are available a statistical approach is needed, which will yield a better approximation for **F**.

Assuming that all particle positions have been measured experimentally, an additional measurement error must be taken into account. The left-hand side of eqn (4) can be rewritten for each pair (P_t, Q_{t_i}) and results in k equations with a right-hand side which equals $\mathbf{d}_i$ $(i \in [1, 2, \ldots, k])$:

$$\mathbf{d}_i = \Delta\mathbf{x}_{t_i} - \mathbf{F}\cdot\Delta\mathbf{x}_{0_i} - {}^3\mathbf{G}:\Delta\mathbf{x}_{0_i}\Delta\mathbf{x}_{0_i} - \mathbf{a} \quad (i \in [1, 2, \ldots, k]). \tag{5}$$

The vectors $\mathbf{d}_i$ represent the sum of the stochastic deviation caused by inherent measurement errors and the random part $\delta\mathbf{a}_i$ of the discretization error. The measurement errors are also assumed to be normally distributed around a constant systematic error. This constant systematic error can be added to $\mathbf{a}$, which then represents the sum of the mean discretization error and the constant systematic measurement error. The remaining deviations $\mathbf{d}_i$ are assumed to be not correlated and normally distributed around the null vector.

The probability density function for the k observed deviations $\mathbf{d}_i$ in a 2D-plane as defined by eqn (5) equals:

$$P[\mathbf{d}_i\,(i \in 1 \ldots k);\mathbf{a};\mathbf{F}] = (2\pi\sigma)^{-k}\,\mathrm{e}^{-\frac{1}{2\sigma^2}\sum_{i=1}^{k}\mathbf{d}_i\cdot\mathbf{d}_i} \tag{6}$$

with $\mathbf{d}_i$ having non-correlated Cartesian components in the x- and y-directions, or

$$\sigma^2 = \sigma_x^2 = \sigma_y^2.$$

Using the maximum likelihood method, the estimates for $\mathbf{F}$, $\mathbf{a}$ and ${}^3\mathbf{G}$ can be retrieved by maximizing the probability density function with respect to the unknown variables ($\mathbf{F}$, $\mathbf{a}$ and ${}^3\mathbf{G}$). Maximizing eqn (6) involves minimizing the scalar function J:

$$J = \sum_{i=1}^{k} \mathbf{d}_i \cdot \mathbf{d}_i$$

or using eqn (5):

$$J = s_{11} - 2\mathbf{F} : \mathbf{W} - 2{}^3\mathbf{G} \vdots {}^3\mathbf{H} - 2\mathbf{m}_t \cdot \mathbf{a} + (\mathbf{F}^c \cdot \mathbf{F}) : \mathbf{X} + 2({}^3\mathbf{G}^c \cdot \mathbf{F}) \vdots {}^3\mathbf{Y} + ({}^3\mathbf{G}^c \cdot {}^3\mathbf{G}) :: {}^4\mathbf{Z} + 2{}^3\mathbf{G} \vdots \mathbf{X}\mathbf{a} + 2\mathbf{F} : \mathbf{m}_0\mathbf{a} + k\mathbf{a} \cdot \mathbf{a}$$

with:

$$s_{11} = \sum_{i=1}^{k} \Delta\mathbf{x}_{t_i} \cdot \Delta\mathbf{x}_{t_i}$$

$$\mathbf{m}_t = \sum_{i=1}^{k} \Delta\mathbf{x}_{t_i}$$

$$\mathbf{m}_0 = \sum_{i=1}^{k} \Delta\mathbf{x}_{0_i}$$

$$\mathbf{X} = \sum_{i=1}^{k} \Delta\mathbf{x}_{0_i}\Delta\mathbf{x}_{0_i}$$

$$\mathbf{W} = \sum_{i=1}^{k} \Delta\mathbf{x}_{0_i}\Delta\mathbf{x}_{t_i}$$

$${}^3\mathbf{H} = \sum_{i=1}^{k} \Delta\mathbf{x}_{0_i}\Delta\mathbf{x}_{0_i}\Delta\mathbf{x}_{t_i}$$

$${}^3\mathbf{Y} = \sum_{i=1}^{k} \Delta\mathbf{x}_{0_i}\Delta\mathbf{x}_{0_i}\Delta\mathbf{x}_{0_i}$$

$${}^4\mathbf{Z} = \sum_{i=1}^{k} \Delta\mathbf{x}_{0_i}\Delta\mathbf{x}_{0_i}\Delta\mathbf{x}_{0_i}\Delta\mathbf{x}_{0_i}.$$

Differentiating J with respect to the unknowns $\mathbf{F}$, $\mathbf{a}$ and ${}^3\mathbf{G}$, and setting the result equal to zero minimizes J which leads to a system of equations for the maximum likelihood estimates $\hat{\mathbf{F}}$ for $\mathbf{F}$, ${}^3\hat{\mathbf{G}}$ for ${}^3\mathbf{G}$ and $\hat{\mathbf{a}}$ for $\mathbf{a}$:

$$\frac{\partial J}{\partial \mathbf{F}} = 0 \Rightarrow -\mathbf{W} + \mathbf{X} \cdot \hat{\mathbf{F}}^c + {}^3\mathbf{Y} : {}^3\hat{\mathbf{G}}^c + \mathbf{m}_0\hat{\mathbf{a}} = \mathbf{O} \tag{8}$$

$$\frac{\partial J}{\partial {}^3\mathbf{G}} = 0 \Rightarrow -{}^3\mathbf{H} + {}^3\mathbf{Y}^c \cdot \hat{\mathbf{F}}^c + {}^4\mathbf{Z} : {}^3\hat{\mathbf{G}}^c + \mathbf{X}\hat{\mathbf{a}} = {}^3\mathbf{O} \tag{9}$$

$$\frac{\partial J}{\partial \mathbf{a}} = 0 \Rightarrow -\mathbf{m}_t + \hat{\mathbf{F}} \cdot \mathbf{m}_0 + {}^3\hat{\mathbf{G}} : \mathbf{X} + k\hat{\mathbf{a}} = \mathbf{O}. \tag{10}$$

By eliminating $\hat{\mathbf{a}}$ from the eqns (8)–(10) the system can be simplified to:

$$\mathbf{A}\cdot\hat{\mathbf{F}}^c + {}^3\mathbf{B}:{}^3\hat{\mathbf{G}}^c = C \tag{11}$$

$${}^3\mathbf{B}^c\cdot\hat{\mathbf{F}}^c + {}^4\mathbf{D}:{}^3\hat{\mathbf{G}}^c = {}^3\mathbf{E} \tag{12}$$

with:

$$\mathbf{A} = k\mathbf{X} - \mathbf{m}_0\mathbf{m}_0$$

$${}^3\mathbf{B} = k^3\mathbf{Y} - \mathbf{m}_0\mathbf{X}^c$$

$$\mathbf{C} = k\mathbf{W} - \mathbf{m}_0\mathbf{m}_t$$

$${}^4\mathbf{D} = k^4\mathbf{Z} - \mathbf{X}\mathbf{X}^c$$

$${}^3\mathbf{E} = k^3\mathbf{H} - \mathbf{X}\mathbf{m}_t.$$

The solution of the system of eqns (11)–(12) finally results in:

$$\hat{\mathbf{F}} = \mathbf{N}^c\cdot\mathbf{M}^{-c} \tag{13}$$

where

$$\mathbf{M} = \mathbf{A} - {}^3\mathbf{B}:{}^4\mathbf{D}^{-1}:{}^3\mathbf{B}^c$$

$$\mathbf{N} = \mathbf{C} - {}^3\mathbf{B}:{}^4\mathbf{D}^{-1}:{}^3\mathbf{E}.$$

Strains can now easily be computed by selecting an adequate strain tensor. In this analysis, the Green–Lagrange strain tensor will be used throughout all computations. The estimate for this tensor is given by:

$$\hat{\boldsymbol{\varepsilon}} = \tfrac{1}{2}(\hat{\mathbf{F}}^c\cdot\hat{\mathbf{F}} - \mathbf{I}). \tag{14}$$

A regular solution of eqn (13) requires regular tensors $\mathbf{M}$ and ${}^4\mathbf{D}$. This condition is satisfied if at least six independent particles, delivering 12 displacement components, are used. These 12 components are required to solve the equations for the unknown six components of ${}^3\mathbf{G}$, the four components of $\mathbf{F}$ and the two components of $\mathbf{a}$. If $\mathbf{a}$ is excluded from the analysis, only five independent particles are needed for a regular solution.

3.2. *Retrieval of the linear model*

The equations for the linear model (Peters, 1987) can be easily retrieved by removing ${}^3\mathbf{G}$ from the eqn (7). The third-order tensors ${}^3\mathbf{H}$, ${}^3\mathbf{Y}$ as well as the fourth-order tensor ${}^4\mathbf{Z}$ then vanish. Equation (9) is no longer relevant, and only the substitution of eqn (10) into eqn (8) is conserved (eqn (11)). Removing ${}^3\mathbf{G}$ from eqn (11) directly leads to the linear solution:

$$\mathbf{A}\cdot\hat{\mathbf{F}}^c = \mathbf{C}$$

or

$$(k\mathbf{X} - \mathbf{m}_0\mathbf{m}_0)\cdot\hat{\mathbf{F}}^c = k\mathbf{W} - \mathbf{m}_0\mathbf{m}_t$$

$$\left(k\sum_i \Delta\mathbf{x}_{0_i}\Delta\mathbf{x}_{0_i} - \mathbf{m}_0\mathbf{m}_0\right)\cdot\hat{\mathbf{F}}^c = k\sum_i \Delta\mathbf{x}_{0_i}\Delta\mathbf{x}_{t_i} - \mathbf{m}_0\mathbf{m}_t. \tag{15}$$

4. ACCURACY ASSESSMENT OF THE GRADIENT DEFORMATION MODEL

4.1. *Numerical simulations*

For an accuracy assessment of the two approaches, a method is required which focuses on the inherent deterministic model error.

The tests used for the comparison, have been chosen such that a 2D-spatial particle distribution has been utilized that approximately matches the 2D-marker distribution of existing experiments based on the Hentschel Random Access Tracking system (Zamzow, 1990). With aid of these quantitative assessments a global, qualitative picture can be obtained of the model error for general strain distributions. All simulations have been performed on an almost square subarea of 11 by 11 points. The entire zone of 121 points covers an area of 3 by 3 cm. The distance between points is thus approximately 3 mm.

In some simulations, the stochastic variation of the distance between the particles (observed in experiments) is also taken into account by scattering the particles around their mean position with a normal distribution. It will be shown that this has a considerable influence on the final results.

The error analysis that is the subject of subsection 4.3, only concerns the model error and not the measurement error which is the subject of a statistical approach.

4.2. *Analytical test fields*

To analyze the performance of both methods five displacement fields with their accompanying strain fields have been adopted:

(i) A constant homogeneous strain field
(ii) A quasi-linear ε_{yy} strain field
(iii) A quasi-quadratic ε_{yy} strain field
(iv) A linear shear strain field
(v) A higher-order complex strain.

The first three fields have been simulated on two different particle distributions:

—A regular distribution with a distance between points of 3 mm. This distribution consists of a perfectly square 11×11 particle field covering the test area of 3×3 cm. The x- and y-distances between the particles are fixed and equal to 3 mm.
—An irregular distribution with a mean distance between particles of 3 mm. This distribution simulates the stochastic deviations of the distances between the particles. The x- and y-distances are normally distributed around a mean value of 3 mm.

The shear strain field and the complex strain field have been tested only on irregular distributions.

4.3. *Evaluation of the strain models*

To compute the approximated strain field from a discrete displacement field, strain groups have to be defined. A strain group is the set of material particles, which surround the central particle in which the strains are to be computed, and is used in the theoretical model to carry out the strain estimation. More particles in a strain group will give better results. Yet, if the distances between the central particle (or marker) and the surrounding particles become large, the remaining discretization error rises significantly and will adversely influence the computational results. In a square particle pattern, three types of particles can be distinguished. The particles in the midfield have neighbouring particles in all directions. The edge markers have neighbours on one side, while the corner markers limit neighbours to a quadrant. The strain groups used in this simulation have eight surrounding particles in the midfield, six at the edges, and five in the corners as illustrated in Fig. 3.

The spatial composition of a strain group influences the quantitative results, but has no real impact on the qualitative interpretation and the comparison between the two models. The specific selection of strain groups used in these simulations is made by comparison of several combinations of strain groups. The current selection mainly involves the particles in the immediate neighbourhood. This selection gives best results in noise-free computations. Some small modifications are recommended, when dealing with noisy data which will be discussed in subsection 4.4.

The simulation of a constant homogeneous strain field is a straightforward test. In this case, both models should reproduce exactly the imposed analytical strain field. It is used to

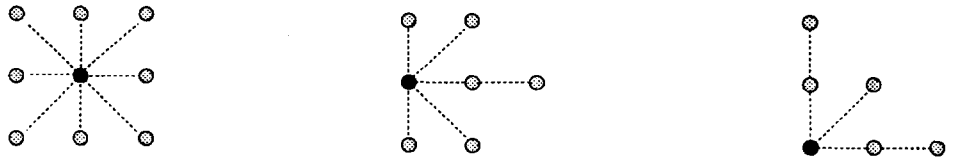

Midfield particle
Strain group (8)

Edge particle
Strain group (6)

Corner particle
Strain group (5)

Fig. 3. Defined strain groups in simulations.

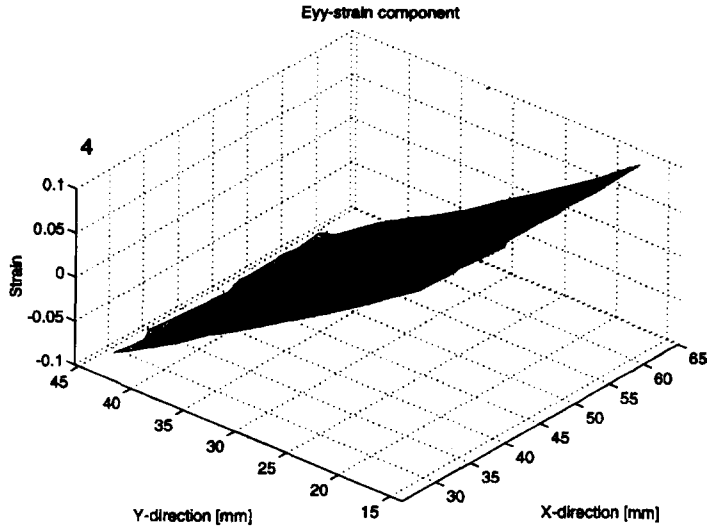

Fig. 4. Analytical exact strain field.

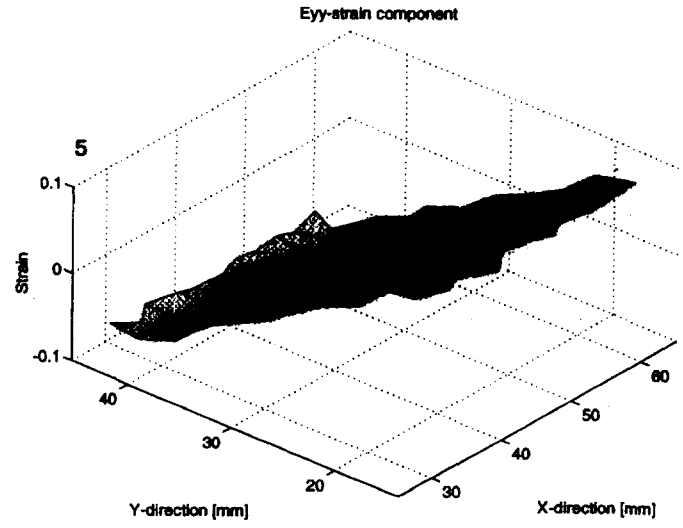

Fig. 5. Computed strain field—linear method.

check possible implementation faults. Both models satisfied this test perfectly. Figures 4–6 illustrate the poor quality of a linear approach in irregular meshes and particularly close to the edges and corners for a quasi-linear strain field. The same conclusion can be drawn from Table 1, which represents the errors relative to the maximum equivalent strain in the entire field. However, the regular distribution gives quasi-zero errors in the midfield. Discretization errors compensate each other, through their regular spatial distribution in a

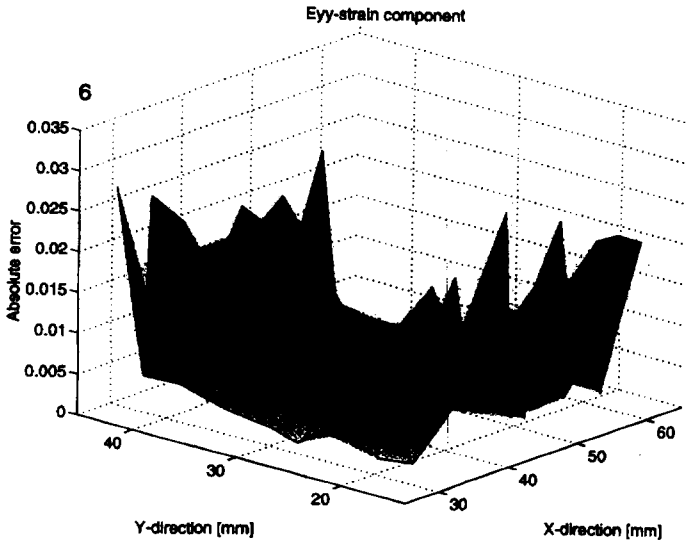

Fig. 6. Theoretical absolute error—linear method.

Table 1. Relative errors on equivalent strain—distance between particles of 3 mm

Simulation results: Computed errors, relative to the maximum strain						
Simulated strain fields		Particle zone	Linear approach		Gradient def. approach	
			Mean (%)	Max (%)	Mean (%)	Max (%)
Linear case $\varepsilon_{eq_{max}}=0.117$	Regular	Midfield	0.0	0.0	0.0	0.0
		Edges	8.9	19.1	0.0	0.0
		Corners	19.6	21.5	0.0	0.0
		Global	3.3	21.5	0.0	0.0
	Irregular	Midfield	3.6	10.1	0.0	0.0
		Edges	10.0	26.8	0.0	0.0
		Corners	18.1	22.6	0.0	0.0
		Global	6.0	26.8	0.0	0.0
Quadratic case $\varepsilon_{eq_{max}}=0.253$	Regular	Midfield	1.1	1.2	1.1	1.2
		Edges	15.3	29.4	1.8	2.5
		Corners	32.8	32.8	2.5	2.5
		Global	6.4	32.8	1.4	2.5
	Irregular	Midfield	2.3	13.4	1.1	1.5
		Edges	16.1	44.0	1.8	4.9
		Corners	33.3	43.4	1.8	3.8
		Global	7.4	44.0	1.3	4.9
Linear shear $\varepsilon_{eq_{max}}=0.164$	Irregular	Midfield	1.6	4.1	0.0	0.0
		Edges	4.7	12.0	0.0	0.0
		Corners	10.7	14.1	0.0	0.0
		Global	2.8	14.1	0.0	0.0
Complex field $\varepsilon_{eq_{max}}=0.051$	Irregular	Midfield	3.5	15.1	2.5	5.9
		Edges	11.2	4.4	1.6	4.5
		Corners	15.3	26.3	1.4	2.4
		Global	6.1	40.4	2.2	5.9

linear field as depicted in Fig. 3. The enhanced higher-order approach perfectly simulates this linear strain field for all spatial particle distributions. Table 1 clearly shows the zero error that is obtained in the midfield, in the edges as well as in the corners. This result could be expected since the order of the chosen discretization scheme corresponds to the order of the displacement field.

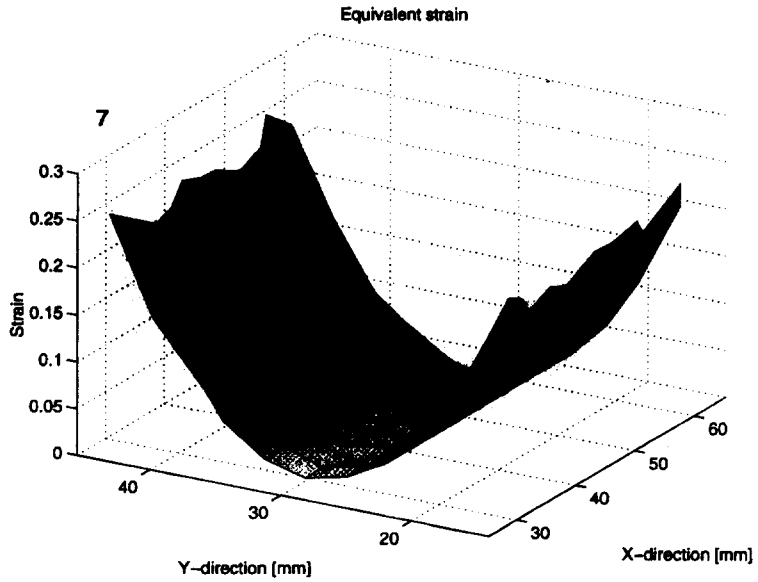

Fig. 7. Analytical exact quadratic strain field.

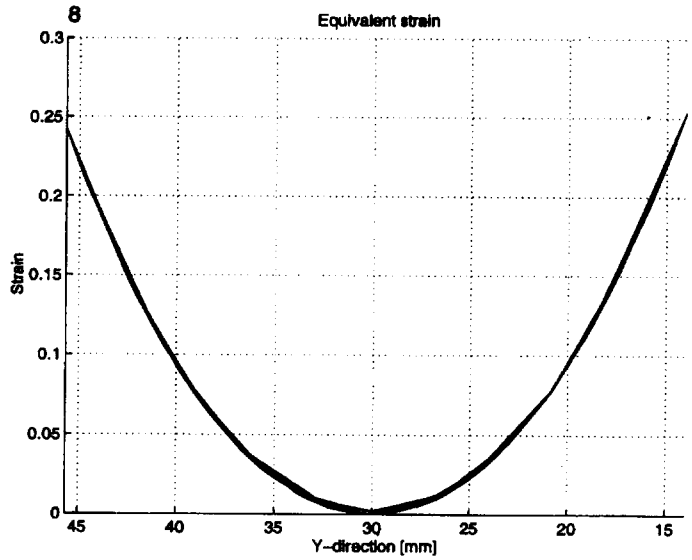

Fig. 8. Side view of the analytical exact strain field for quadratic strain distribution.

Figure 7 shows the exact equivalent strain ε_{eq} (equal to ε_{yy}) of a quadratic strain, where the equivalent strain is defined as:

$$\varepsilon_{eq} = \sqrt{\varepsilon_{xx}^2 + \varepsilon_{yy}^2 + 2\varepsilon_{xy}^2}.$$

When the quadratic 3D-shape is projected on a 2D-plane with normal along the X-axis, the parabolic curve of Fig. 8 is obtained.

Both approaches will now be tested with this quadratic strain field. The linear model produces a strain field, which is shown in Fig. 9. The numerically simulated field is superimposed on the analytical solution, so as to enhance the contrast. The model error becomes large close to the boundaries of the particle mesh. Even in the midfield, computed strains deviate significantly from their correct values. These examples show, once more, that the linear model is sensitive to the spatial particle distribution, and cannot produce reliable results close to the edges nor in the midfield of inhomogeneous strain fields. The error on

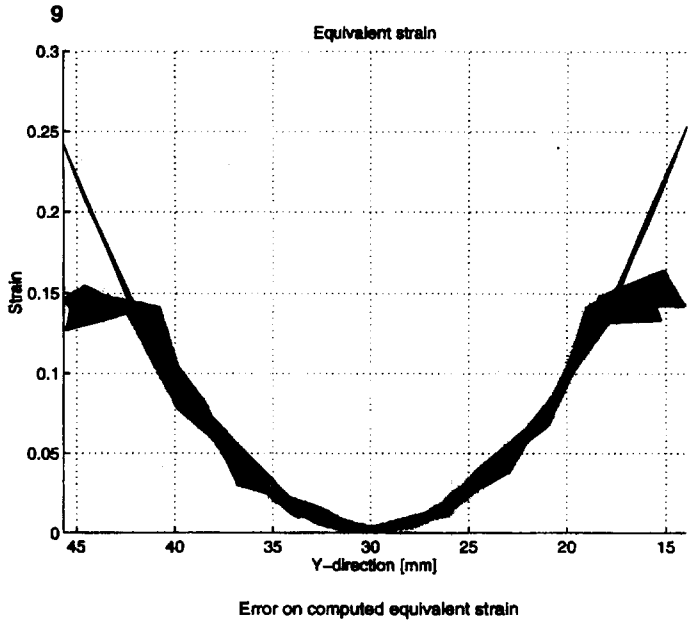

Error on computed equivalent strain

Fig. 9. Comparison between analytical and computed strain field (linear model).

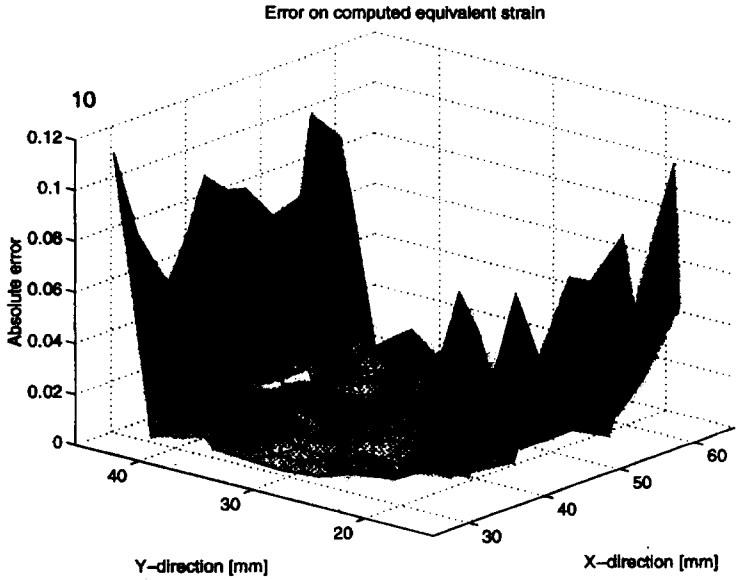

Fig. 10. Error on the computed strain field (linear model).

the equivalent strain is depicted in Fig. 10. The large errors at the edges are striking. The same conclusions can be reached when analyzing Table 1. All errors are relative to the maximum equivalent strain in the strain field. The values of these maximum effective equivalent strains are listed in the first column of Table 1.

The gradient deformation model constitutes a substantial improvement. The 2D-view of the computed equivalent strain field and the analytical correct solution, analogous to Fig. 9, is shown in Fig. 11. The approximation is excellent, even at the boundaries and at the corners of the particle field. The accompanying error plot in Fig. 12 is represented using the same scale as in Fig. 10.

Table 1 shows that the strains cannot be predicted correctly from an irregular displacement grid when using the linear model. Regular distributions do not produce reliable results with the linear model if non-linear variations exist in the strain field. The mean relative error for the quadratic strain field with a regular grid reduces from 6.4% for the

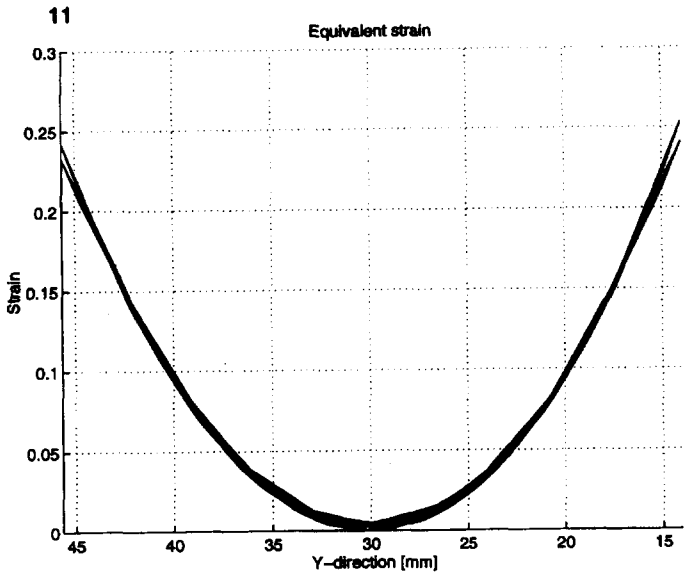

Fig. 11. Comparison between analytical and computed strain field (gradient deformation model).

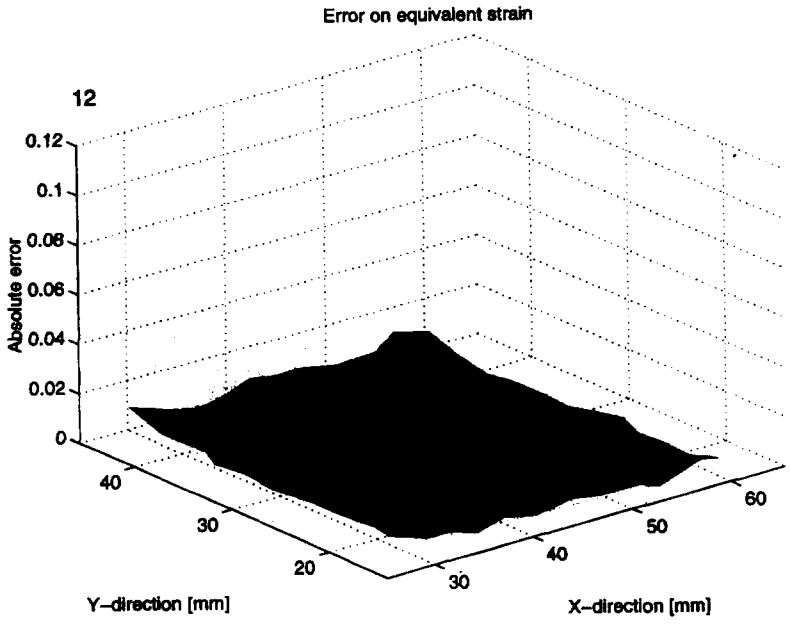

Fig. 12. Error on the computed strain field (gradient deformation model).

linear model to 1.4% for the gradient deformation model, while the maximum relative error is reduced from 32.8% to 2.5%.

A simulation with a linear shear strain distribution leads to the same conclusions. Another interesting example is offered by a more complex strain field. This strain field has an embedded highly strained zone which is of particular interest in localization problems. The maximum equivalent strain in the midfield is about 0.051. The errors in the prediction computed with the linear model are given in Table 1. Again, the errors at the edges and corners are obvious. Clearly, the strains at the edges and the corners are much more accurate for the gradient deformation model. Even in the midfield, the maximum error is reduced from 15.1% to 5.9%. However, the gain in precision is smaller than in the preceding simulations. If the local gradient is too strong for the chosen discretization, a second-order scheme may be insufficient and the discretization must be refined.

Edge particle
Strain group (8)

Corner particle
Strain group (8)

Fig. 13. Enhanced strain groups near edges and corners for noisy displacements.

4.4. *Comparing results computed on corrupted data*

Experimental data are always corrupted by noise. An efficient strain computation requires preliminary filtering of the corrupted displacement signals. The present analysis of non-correlated white noise, and the filtering procedure to eliminate it, is based on the singular value decomposition (SVD). It has been shown by many authors (Deprettere, 1988; Muijtens *et al.*, 1990) that the singular value decomposition is an efficient tool to accomplish this task. Many valuable properties of the singular value decomposition, including existence proofs, numerical considerations and sensitivity results can be found in Golub and Loan (1983). Without noise reduction, high noise levels lead to measurement errors which supersede the model errors. Using a good filtering scheme, the random noise on input signals can be reduced significantly, limiting the influence of the experimental errors. A proper error analysis requires a statistical prediction of the confidence intervals for the measured physical property. Such an analysis was carried out by Peters (1987) for the linear model. However, the gradient deformation model is not well suited for a straightforward statistical analysis because of the complexity of its mathematical formulation. In many cases, the linear approach presents a very significant model error, exceeding any statistical prediction towards the expected value of the strains.

To treat data more efficiently close to edges and corners and to improve statistical weighting (in spite of a small decrease in model precision), the strain groups in edges and corners, used in the gradient deformation model, are slightly modified. These enhanced strain groups, shown in Fig. 13, use eight neighbouring particles instead of five and six, respectively.

Using similar simulations as presented above, the model error appears to be the most relevant contribution in almost all practical cases. The imposed displacement fields have been perturbed by a normally distributed random noise signal. The variance of this noise signal has been chosen equal to the noise variance that has been observed in associated experiments. The linear and gradient deformation model have been used to compute strains after the filtering procedures. The results of these simulations are summarized in Table 2 and Table 3. Table 2 shows the mean relative errors on the computed noisy strain fields, while Table 3 lists the maximum relative errors.

A first simulation concerns a constant homogeneous strain field. When noise-free, such a strain field is correctly described by both models with a zero model error. In the presence of noise corruption (simulating measurement errors), the linear model gives more accurate results than the gradient deformation model (mean and maximum error). This can be expected, since it has been stipulated before that the statistical weighting in the higher-order model is less efficient than in the linear case. In most cases, the model error for the linear model is so important that the addition of noise does not result in substantial changes of the computed errors. Relative to the theoretical model precision, the gradient deformation model is more sensitive to noise, and requires good filtering. Enlargement of the strain groups does not solve this problem, because of the negative effect on the discretization error due to the increase of the particle distances.

All other simulations lead to conclusions which favour the use of the gradient deformation model. Regular grids with the linear model give mean errors in the midfield which equal those by the gradient deformation model. The regular spatial distribution forces a model error compensation between the different particles. This artificial error compensation

Table 2. Mean relative errors on equivalent strain—computed from a noisy displacement field

Simulation results: Computed mean errors, relative to the maximum strain						
Simulated strain fields		Particle zone	Linear approach		Gradient def. approach	
			Noise-free (%)	Noise (%)	Noise-free (%)	Noise (%)
Constant case $\varepsilon_{eq_{max}} = 0.094$	Regular	Midfield	0.0	1.0	0.0	1.0
		Edges	0.0	1.2	0.0	1.9
		Corners	0.0	1.6	0.0	2.2
		Global	0.0	1.1	0.0	1.3
	Irregular	Midfield	0.0	0.9	0.0	1.3
		Edges	0.0	1.2	0.0	2.0
		Corners	0.0	1.8	0.0	2.4
		Global	0.0	1.0	0.0	1.5
Linear case $\varepsilon_{eq_{max}} = 0.117$	Regular	Midfield	0.0	0.8	0.0	0.8
		Edges	8.9	8.8	0.0	1.6
		Corners	19.6	18.6	0.0	1.4
		Global	3.3	3.8	0.0	1.1
	Irregular	Midfield	3.7	3.8	0.0	1.1
		Edges	10.7	10.3	0.0	1.6
		Corners	19.1	18.0	0.0	1.4
		Global	6.3	6.2	0.0	1.3
Quadratic case $\varepsilon_{eq_{max}} = 0.118$	Regular	Midfield	1.2	1.3	1.2	1.3
		Edges	15.3	15.4	1.8	2.1
		Corners	32.7	33.3	2.4	2.9
		Global	6.4	6.5	1.4	1.6
	Irregular	Midfield	3.4	3.5	1.1	1.4
		Edges	16.6	16.7	1.8	2.3
		Corners	32.3	32.9	2.2	3.4
		Global	8.3	8.4	1.4	1.8
Complex field $\varepsilon_{eq_{max}} = 0.104$	Irregular	Midfield	5.1	5.1	2.5	2.4
		Edges	12.8	12.8	2.0	3.0
		Corners	21.0	20.2	5.5	8.6
		Global	7.9	7.9	2.5	2.8

vanishes in irregular grids. In real experiments, regular grids cannot be realized since some random irregularity will always be present. It is particularly interesting to notice that especially the maximum error is diminished by the higher-order approach. These practical examples, computed from noisy data, show that the preceding conclusions made from noise free simulations in subsection 4.2 remain valid. In sum, the linear model is recommended only if no strain variations are expected. However, the determination of a constant strain field can be accomplished easier by other techniques (LVDTs, strain gauges, ...).

5. CONCLUDING REMARKS

A methodology has been proposed to compute strains from discrete sets of displacements, which have been obtained using experimental techniques like Electronic Speckle Pattern Interferometry (ESPI) (see Bergmann *et al.*, 1995 or Galanulis and Ritter, 1993 for more details), or using the Hentschel Random Access Tracking System (Zamzow, 1990). Two possibilities have been explored, namely an existing method (Peters, 1987) in which the variation in the local displacement field is truncated after the linear terms (first-order method), and a new approach (second-order method) in which quadratic terms are also included in the variation of the local displacement field. A comparison on a number of test cases with prescribed, known strain fields clearly shows the superiority of the second-order method. The superiority of the higher-order approach diminishes somewhat if corruption of the displacement signals is taken into account, especially for slowly varying strain distributions. However, for cases with high strain gradients such as typically occur in localization problems, the use of the higher-order approach is clearly advantageous.

Table 3. Maximum relative errors on equivalent strain—computed from a noisy displacement field

Simulation results: Computed maximum errors, relative to the maximum strain						
Simulated strain fields		Particle zone	Linear approach		Gradient def. approach	
			Noise-free (%)	Noise (%)	Noise-free (%)	Noise (%)
Constant case $\varepsilon_{eq_{max}} = 0.094$	Regular	Midfield	0.0	3.0	0.0	3.0
		Edges	0.0	4.1	0.0	5.7
		Corners	0.0	3.0	0.0	4.0
		Global	0.0	4.1	0.0	5.7
	Irregular	Midfield	0.0	3.0	0.0	5.9
		Edges	0.0	3.6	0.0	5.1
		Corners	0.0	2.4	0.0	4.1
		Global	0.0	3.6	0.0	5.9
Linear case $\varepsilon_{eq_{max}} = 0.117$	Regular	Midfield	0.0	2.5	0.0	2.5
		Edges	19.1	21.5	0.0	7.4
		Corners	21.5	22.5	0.0	2.7
		Global	21.5	22.5	0.0	7.4
	Irregular	Midfield	9.7	10.3	0.0	5.1
		Edges	24.0	26.1	0.0	7.2
		Corners	23.2	21.3	0.0	2.4
		Global	24.0	26.1	0.0	7.2
Quadratic case $\varepsilon_{eq_{max}} = 0.118$	Regular	Midfield	1.2	2.9	1.2	2.9
		Edges	29.2	32.3	2.5	7.5
		Corners	32.7	34.7	2.5	4.5
		Global	32.7	34.7	2.5	7.5
	Irregular	Midfield	11.6	10.6	1.7	4.9
		Edges	38.1	39.0	3.9	8.8
		Corners	39.7	41.1	3.0	5.0
		Global	39.7	41.1	3.9	8.8
Complex field $\varepsilon_{eq_{max}} = 10.4$	Irregular	Midfield	15.2	15.7	7.3	7.2
		Edges	41.6	38.8	6.1	8.1
		Corners	41.8	40.2	10.6	13.3
		Global	41.8	40.2	10.6	13.3

Another advantage is that in the second-order approach all particles can be taken into account for the strain computation. Errors at edges and at corners then have approximately the same error magnitude as in the midfield, as a consequence, strain distributions around internal boundaries such as cracks can be determined much more accurately.

REFERENCES

Bergmann, D., Galanulis, K., Ritter, R. and Winter, D. (1995). Application of optical field methods in material testing and quality control, electronic speckle pattern interferometry and grating method. In *Photomécanique 95*, pp. 257–265. Edition Eyrolles.

de Borst, R., Sluys, L., Mühlhaus, H.-B. and Pamin, J. (1993). Fundamental issues in finite element analysis of localisation of deformation. *Engng Computations* **10**, 99–122.

Deprettere, F. (editor) (1988). *SVD and Signal Processing—Algorithms, Applications and Architectures*. Elsevier Science Publishers B.V.

Galanulis, K. and Ritter, R. (1993). Speckle interferometry in material testing and in dimensioning of structures. *SPIE* **2004**, Interferometry VI: Applications, 269–275.

Golub, G. and Loan, C. V. (1983). *Matrix Computations*, North Oxford Academic/Johns Hopkins University Press.

Hunter and Zerhouni (1989). Imaging distinct points in left ventricular myocardium to study regional wall deformation. *Innovations in Diagnostic Radiology* (Edited by J. Anderson), pp. 169–190. Springer-Verlag, Berlin.

Muijtens, A., Prinzen, J., Hasman, T., Reneman, A. and Arts, R. (1990). Noise reduction in estimating cardiac deformation from marker tracks. In *Special Communications*. American Physiological Society.

Peters, G. (1987). Tools for the measurement of stress and strain fields in soft tissue. PhD thesis, Eindhoven University of Technology.

Zamzow, H. (1990). The Hentschel Random Access Tracking System hsg 84.30. *SPIE* **1356**, 130–133.